 CMES, vol.67, no.2, pp.151-173, 2010

A Comprehensive Finite Element Model for Tapered Composite Wing Structures

Chyanbin Hwu[1,2] **and Mengchun Yu**[1]

Abstract: A comprehensive finite element model incorporating the features of comprehensive wing model and finite element method is developed in this paper. This new model extends the applicability of comprehensive wing model from uniform composite wings to tapered composite wings. It preserves the simplicity of one-dimensional finite element but performs like three-dimensional finite element for wing structural analysis. To verify its accuracy and show its efficiency, this model which is applicable to the general dynamic analysis is reduced to two simple cases: static analysis and free vibration analysis. Based upon the reduction results for static and free vibration cases, several numerical examples of composite wing structures are presented such as tapered wings subjected to end load or uniform pressure, and free vibration of tapered wings. The numerical results show that the proposed model is much more efficient than the conventional finite element, and their differences are within 12% in all cases of composite wing structures.

1 Introduction

To study the mechanical behavior of composite wing structures, several different structural models have been proposed in the literatures such as the classical beam model [Bisplinghoff, Asheley, and Halfman (1955); Megson (1990); Vinod, Gopalakrishnan, and Ganguli (2006)], the box beam model [Weisshaar and Foist (1985); Chandra, Stemple, and Chopra (1990); Banerjee and Williams (1995)], the refined model considering the warping restraint [Crawley and Dugundji (1980); Lottati (1985); Librescu and Khdeir (1988); Oyibo and Bentson (1990)] and/or transverse shear deformation [Librescu and Song (1992)] and/or shell bending strain [Volovoi and Hodges (2002); Volovoi and Hodges (2000)] and/or cross-sectional materials and geometries [Yu, Volovoi, Hodges, and Hong (2002); Yu, Hodges,

[1] Institute of Aeronautics and Astronautics, National Cheng Kung University, Tainan, Taiwan, R.O.C.

[2] Corresponding author. Tel: 886-6-2757575 ext.63662; Fax: 886-6-2389940; E-mail: CHwu@mail.ncku.edu.tw

Volovoi, and Cesnik (2002); Sapountzakis and Tsiatas (2007)], and the comprehensive wing model considering the shape of airfoil [Hwu and Tsai (2002); Hwu and Gai (2003)]. However, due to the mathematical complexity, most of the wing models assume that the cross section of the wing is uniform in spanwise direction, and therefore cannot be applied to study the tapered wings. Only the simple models such as the box beam model [Weisshaar (1980)] and the refined model [Librescu and Simovich (1988); Vadiraja and Sahasrabudhe (2008)] considered the taper effects.

In order to preserve the essential features of the comprehensive wing models and to avoid the mathematical complexity raised by the taper effects, a comprehensive finite element model (CFEM) is proposed in this paper. To build a good connection between the analytical model and finite element model, the matrix form comprehensive wing model proposed in [Hwu and Gai (2003)] is re-derived in this paper by using the Hamilton's principle [Reddy (1993)]. In this re-derivation, all the basic functions are unknowns and will be determined by solving the ordinary differential equation together with its associated boundary and initial conditions. With the concept of finite element method, the unknown basic functions were assumed to have unknown values only at the nodal points of each element. By combining this assumption for finite element method, the comprehensive wing model is then extended to be CFEM.

CFEM combines the merits of analytical models and numerical models. In conventional finite element model only displacements and/or rotations are selected as nodal displacements, whereas in CFEM the nodal displacements include all the basic functions of the comprehensive wing model [Hwu and Tsai (2002); Hwu and Gai (2003)], i.e., the vertical deflection, the displacement in spanwise direction, the twist angle, the rotation angle, and the rate of angle change. With the enhancement of the nodal degree of freedom, CFEM still preserves the simplicity of one-dimensional finite element but performs like three-dimensional finite element for wing structural analysis. Moreover, since CFEM is developed based upon the comprehensive wing model, in this paper it has been shown to be more efficient than the conventional finite element model. Its accuracy is verified through the comparison with the analytical solutions for uniform wings and the numerical solutions obtained by the commercial finite element software ANSYS.

2 Comprehensive Wing Model

In the previous studies of our co-workers [Hwu and Tsai (2002); Hwu and Gai (2003)], a matrix form comprehensive analytical model was developed to analyze the composite wing structures. In that model, the entire wing structure is simulated by a composite sandwich plate with variable thickness. The wing skin made

of composite laminates together with stringers and spar flanges are simulated as the faces resisting the in-plane force and bending moment, whereas the spar webs and ribs are simulated as the core resisting the transverse shear force. According to the chordwise-rigid postulation [Megson (1990)], the displacement field of the composite wings is assumed as [Hwu and Tsai (2002)]

$$\begin{aligned} u(x,y,z,t) &= z\theta(y,t), \\ v(x,y,z,t) &= v_0(y,t)+z\{\beta_f(y,t)+x\beta_r(y,t)\}, \\ w(x,y,z,t) &= w_f(y,t)-x\theta(y,t), \end{aligned} \tag{1}$$

where u, v, w are the displacement components in the directions of x (chordwise), y (spanwise) , and z (thicknesswise), respectively (see Fig. 1). t denotes the time variable. v_0 is the mid-plane displacements in y direction. w_f denotes the vertical deflection (positive upward) measured at the line of the reference axis; θ is the rotation angle with respect to x-axis due to the twist around the reference axis (positive nose up), i.e., $\beta_x = \theta$. β_f denotes the rotation angle with respect to y axis measured at the reference axis and β_r stands for the rate of angle change in the x-direction. Thus, $\beta_y = \beta_f + x\beta_r$.

According to the postulation in Eq. (1), the basic functions describing the deformation of the stiffened composite wing structures become v_0, w_f, θ, β_f, and β_r. With these five basic functions, the equations of motion governing composite wings can

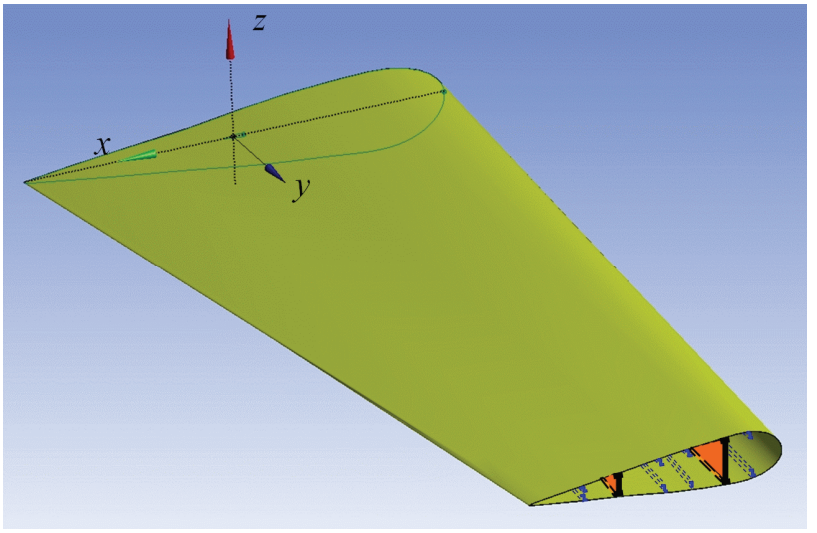

Figure 1: Tapered composite wings.

be written as [Hwu and Gai (2003)]

$$\mathbf{K}_2\boldsymbol{\Delta}''(y,t)+(\mathbf{K}_1-\mathbf{K}_1^T)\boldsymbol{\Delta}'(y,t)-\mathbf{K}_0\boldsymbol{\Delta}(y,t)+\mathbf{p}(y,t)=\mathbf{I}_0\ddot{\boldsymbol{\Delta}}(y,t). \tag{2}$$

In Eq. (2), the prime $\bullet'$ means differentiation with respect to y; the overdot $\dot{\bullet}$ denotes the time derivative; the superscript T stands for the transpose of a matrix; $\boldsymbol{\Delta}$ and $\mathbf{p}$ are, respectively, the *generalized displacement* and *load vector*; $\mathbf{K}_0$, $\mathbf{K}_1$ and $\mathbf{K}_2$ are three *stiffness matrices*, $\mathbf{I}_0$ is an *inertia matrix* related to the mass, center of gravity, and moment of inertia, which are defined as

$$\boldsymbol{\Delta}=\begin{Bmatrix} v_0 \\ w_f \\ \theta \\ \beta_f \\ \beta_r \end{Bmatrix},\ \mathbf{p}=\begin{Bmatrix} \tilde{p}_y \\ \tilde{p} \\ \tilde{m}_x-\tilde{p}^* \\ \tilde{m}_y \\ \tilde{m}_y^* \end{Bmatrix}, \tag{3a}$$

$$\mathbf{K}_0=\begin{bmatrix} 0&0&0&0&0 \\ 0&0&0&0&0 \\ 0&0&0&0&0 \\ 0&0&0&\tilde{A}_{44}&\tilde{A}_{44}^* \\ 0&0&0&\tilde{A}_{44}^*&\tilde{D}_{66}+\tilde{A}_{44}^{**} \end{bmatrix},\ \mathbf{K}_1=\begin{bmatrix} 0&0&0&0&\tilde{B}_{26} \\ 0&0&0&\tilde{A}_{44}&\tilde{A}_{44}^* \\ 0&0&0&-\tilde{A}_{44}^*&\tilde{D}_{66}-\tilde{A}_{44}^{**} \\ 0&0&0&0&\tilde{D}_{26} \\ 0&0&0&0&\lambda\tilde{D}_{26}^* \end{bmatrix}, \tag{3b}$$

$$\mathbf{K}_2=\begin{bmatrix} \tilde{A}_{22}&0&\tilde{B}_{26}&\tilde{B}_{22}&\lambda\tilde{B}_{22}^* \\ 0&\tilde{A}_{44}&-\tilde{A}_{44}^*&0&0 \\ \tilde{B}_{26}&-\tilde{A}_{44}^*&\tilde{D}_{66}+\tilde{A}_{44}^{**}&\tilde{D}_{26}&\lambda\tilde{D}_{26}^* \\ \tilde{B}_{22}&0&\tilde{D}_{26}&\tilde{D}_{22}&\lambda\tilde{D}_{22}^* \\ \lambda\tilde{B}_{22}^*&0&\lambda\tilde{D}_{26}^*&\lambda\tilde{D}_{22}^*&\lambda\tilde{D}_{22}^{**} \end{bmatrix},$$

$$\mathbf{I}_0=\begin{bmatrix} m&0&0&mz_c&I_{xz} \\ 0&m&-mx_c&0&0 \\ 0&-mx_c&I_y&0&0 \\ mz_c&0&0&I_x&I_{xz^2} \\ I_{xz}&0&0&I_{xz^2}&I_{x^2z^2} \end{bmatrix}. \tag{3c}$$

In the above, $\tilde{p}_y$, $\tilde{p}$, $(\tilde{m}_x-\tilde{p}^*)$, $\tilde{m}_y$, and $\tilde{m}_y^*$ are the forces corresponding to v_0, w_f, θ, β_f, and β_r; $\tilde{A}_{ij}$, $\tilde{B}_{ij}$, $\tilde{D}_{ij}$, $\tilde{A}_{ij}^*$, $\tilde{B}_{ij}^*$, $\tilde{D}_{ij}^*$, $\tilde{A}_{ij}^{**}$, $\tilde{B}_{ij}^{**}$, $\tilde{D}_{ij}^{**}$, $i,j=1,2,...,6$ are the resultant stiffnesses related to the extensional stiffness A_{ij}, coupling stiffness B_{ij}, and bending stiffness D_{ij} of the composite wings; m is the mass per unit spanwise length; (x_c,z_c) is the coordinate of the center of gravity of cross section whose y=constant; and I_x, I_y, I_{xz}, I_{xz^2}, and $I_{x^2z^2}$ stand for the mass moment of inertia in different directions; λ is a tracer used to identify the warping effect, i.e., $\lambda=0$ for free warping condition and $\lambda=1$ means that the warping restraint is implied.

For the convenience of readers' reference, detailed definitions of these symbols are provided in Appendix A.

Although the Eq. (2) derived by our co-workers [Hwu and Gai (2003)] is a result of comprehensive wing model which considers several effects such as bending-torsion coupling, warping restraint, transverse shear deformation, shape of airfoil, rotary inertia, etc., it cannot be applied to the tapered wings because in this model the wing cross section is considered to be independent of y (spanwise direction). In other words, in Eq. (2) the stiffness and inertia matrices, $\mathbf{K}_0$, $\mathbf{K}_1$, $\mathbf{K}_2$, and $\mathbf{I}_0$ are all constant matrices, which is not true for tapered wings. In order to extend the comprehensive wing model to tapered wings or more general wing cases, a concept like finite element model is adopted in this paper. That is, the tapered wing is cut into several elements and each element is approximated by a uniform wing section. Since the finite element formulation can be established by minimizing the *Lagrangian function* [Reddy (1993)], to have a smooth transition from the comprehensive wing model to comprehensive finite element wing model, we now re-derive Eq. (2) through the use of *Hamilton's principle*. It states that the motion of a continuum acted on by conservative forces between two arbitrary instants of time t_1 and t_2 is such that the line integral over the Lagrangian function is an extremum for the path motion [Reddy (1993)]. The Lagrangian function is the difference between kinetic and total potential energies, and the total potential energy is the sum of the strain energy and potential energy of external forces. Thus, the Hamilton's principle can be expressed by

$$\delta \int_{t_1}^{t_2} (\Pi - T) dt = 0 \tag{4}$$

where δ is the variational operator, t_1 and t_2 are the integration limits of time. Π is the total potential energy and T is the kinetic energy, which can be written as

$$\Pi = \int_V (W - f_i u_i) dV - \int_{S_\sigma} \hat{t}_i u_i dS, \quad T = \frac{1}{2} \int_V \rho \dot{u}_i \dot{u}_i dV, \tag{5}$$

where W, f_i, u_i, and $\hat{t}_i$ are, respectively, the strain energy density, body forces, displacements, and prescribed surface tractions; V and S_σ are the regions for volume and surface integrals, respectively. By performing the integration of the potential and kinetic energy in the sequence of thickness direction (z), chordwise direction (x), and spanwise direction (y), and expressing the results in matrix form, we get (please refer to Appendix B for the details of integration)

$$\Pi - T = \frac{1}{2} \int_y \{\mathbf{F}^T \boldsymbol{\Delta}' + \mathbf{F}_0^T \boldsymbol{\Delta} - 2\mathbf{p}^T \boldsymbol{\Delta} - \dot{\boldsymbol{\Delta}}^T \mathbf{I}_0 \dot{\boldsymbol{\Delta}}\} dy - [\hat{\mathbf{F}}^T \boldsymbol{\Delta}]_{y_1}^{y_2}, \tag{6a}$$

where $\mathbf{F}$ and $\mathbf{F}_0$ are *force vectors* defined by

$$\mathbf{F}=\begin{Bmatrix}\tilde{N}_y\\ \tilde{Q}_y\\ \tilde{M}_{xy}-\tilde{Q}_y^*\\ \tilde{M}_y\\ \tilde{M}_y^*\end{Bmatrix},\ \mathbf{F}_0=\begin{Bmatrix}0\\ 0\\ 0\\ \tilde{Q}_y\\ \tilde{M}_{xy}+\tilde{Q}_y^*\end{Bmatrix}. \tag{6b}$$

In the above, $\hat{\mathbf{F}}$ denotes the prescribed value of $\mathbf{F}$ on the boundary $y=y_1$ or $y=y_2$, which is the integration limits of y, and $[f]_{y_1}^{y_2}=f(y_2)-f(y_1)$; $\tilde{N}_y$, $\tilde{Q}_y$, $\tilde{M}_{xy}$, $\tilde{M}_y$, $\tilde{Q}_y^*$, $\tilde{M}_y^*$ are the resultant forces whose detailed definitions are given in Appendix A.

From the constitutive relations for laminated composite sandwiches, we know that the force vectors $\mathbf{F}$ and $\mathbf{F}_0$ are related to the displacement vector $\boldsymbol{\Delta}$ by [Hwu and Gai (2003)]

$$\mathbf{F}=\mathbf{K}_1\boldsymbol{\Delta}+\mathbf{K}_2\boldsymbol{\Delta}',\ \mathbf{F}_0=\mathbf{K}_0\boldsymbol{\Delta}+\mathbf{K}_1^T\boldsymbol{\Delta}'. \tag{7}$$

Substituting Eq. (8) into Eq. (10), we get

$$\Pi-T=\frac{1}{2}\int_y\{2\boldsymbol{\Delta}^T\mathbf{K}_1^T\boldsymbol{\Delta}'+\boldsymbol{\Delta}'^T\mathbf{K}_2\boldsymbol{\Delta}'+\boldsymbol{\Delta}^T\mathbf{K}_0\boldsymbol{\Delta}-\dot{\boldsymbol{\Delta}}^T\mathbf{I}_0\dot{\boldsymbol{\Delta}}-2\mathbf{p}^T\boldsymbol{\Delta}\}dy-[\hat{\mathbf{F}}^T\boldsymbol{\Delta}]_{y_1}^{y_2} \tag{8}$$

With the result of Eq. (11), the first variation of the Lagrangian, $\Pi-T$, can be obtained as (see Appendix C for the details of variation operation)

$$\begin{aligned}\delta(\Pi-T)=&\int_y(\delta\boldsymbol{\Delta}^T)[(\mathbf{K}_1^T-\mathbf{K}_1)\boldsymbol{\Delta}'-\mathbf{K}_2\boldsymbol{\Delta}''+\mathbf{K}_0\boldsymbol{\Delta}+\mathbf{I}_0\ddot{\boldsymbol{\Delta}}-\mathbf{p}]dy\\&+(\delta\boldsymbol{\Delta}^T)[\mathbf{K}_1\boldsymbol{\Delta}+\mathbf{K}_2\boldsymbol{\Delta}'-\hat{\mathbf{F}}]_{y_1}^{y_2}-\frac{\partial}{\partial t}\int_y(\delta\boldsymbol{\Delta}^T)\mathbf{I}_0\boldsymbol{\Delta}dy.\end{aligned} \tag{9}$$

With the result obtained in Eq. (9), the Hamilton's principle Eq. (4) can then provide the governing equation and boundary conditions as follows,

$$\begin{aligned}&\mathbf{K}_2\boldsymbol{\Delta}''+\left(\mathbf{K}_1-\mathbf{K}_1^T\right)\boldsymbol{\Delta}'-\mathbf{K}_0\boldsymbol{\Delta}+\mathbf{p}=\mathbf{I}_0\ddot{\boldsymbol{\Delta}},\ \text{for all } y,\\&\boldsymbol{\Delta}=\hat{\boldsymbol{\Delta}}\ \text{or}\ \mathbf{K}_1\boldsymbol{\Delta}+\mathbf{K}_2\boldsymbol{\Delta}'=\hat{\mathbf{F}},\ \text{on } y=y_r \text{ and } y=y_t.\end{aligned} \tag{10}$$

where $y=y_t$ or $y=y_r$, which are the locations of wing tip or wing root. Equation (10) is the same as that shown in Eq. (2) derived by different approach in [Hwu and Gai (2003)].

3 Comprehensive Finite Element Model

As stated previously in the paragraph between Eqns.(3c) and (4), the comprehensive wing model cannot be applied to the tapered wings directly. In order to extend its applicability to the case of tapered wings, a comprehensive dynamic finite element model is introduced in this section. By this new model, the tapered wings will be divided into a series of elements which are connected at a finite number of nodal points. The cross section is assumed to be uniform in spanwise direction (y-direction) within each element as shown in Fig. 2. Since the cross section can be different for different element, general wing shapes including tapered wings can be handled through this new model.

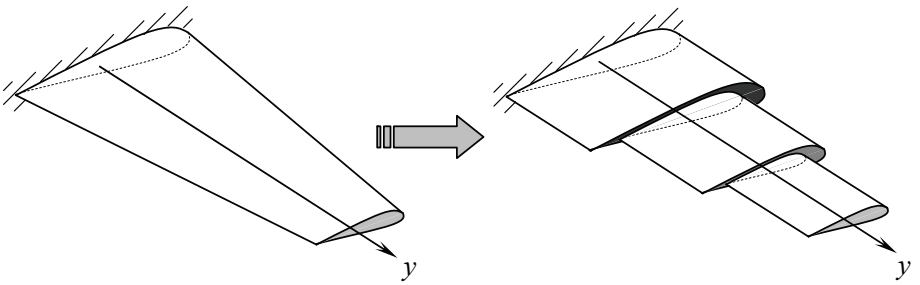

Figure 2: Discretization of the tapered wings.

In the finite element displacement method, the displacement is assumed to have unknown values only at the nodal points, so that the variation within any element is described in terms of the nodal values by means of interpolation function. With this understanding, within each element the generalized displacement vector $\mathbf{\Delta}$ composed of five basic functions $v_0,\ w_f,\ \theta,\ \beta_f$, and β_r is now assumed as

$$\mathbf{\Delta} = g(t)\mathbf{N}(y)\mathbf{u}_e, \tag{11}$$

where, $\mathbf{u}_e$ is a 15×1 vector of nodal displacements of the element, $\mathbf{N}(y)$ is a 5×15 matrix containing a set of shape functions, and $g(t)$ is a time function assumed to be the same for all degrees of freedom.

In this paper, each element is assumed to have three nodal points as shown in Fig. 3 and each basic function is assumed to be interpolated by the same shape functions

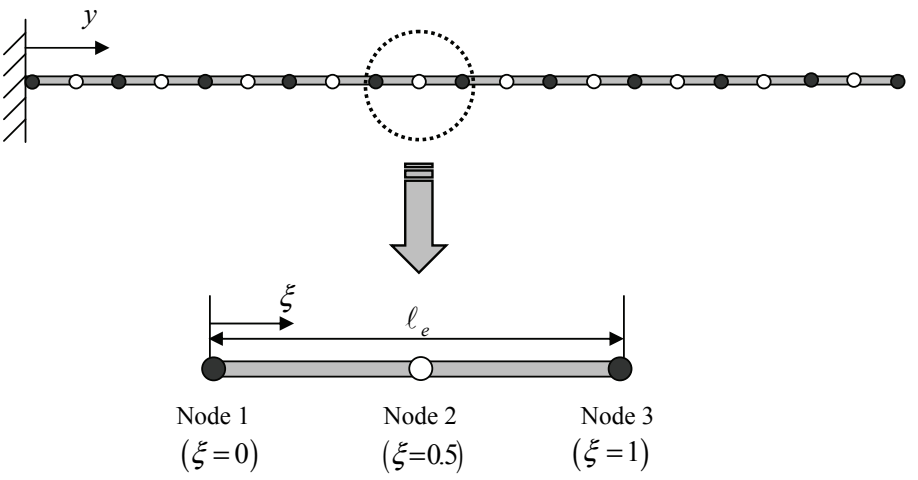

Figure 3: Finite element discretization and element local coordinate.

within element. Thus, $\mathbf{u}_e$ and $\mathbf{N}(y)$ can be written in a partition form as

$$\mathbf{u}_e = \begin{Bmatrix} \boldsymbol{\Delta}_1 \\ \boldsymbol{\Delta}_2 \\ \boldsymbol{\Delta}_3 \end{Bmatrix}, \boldsymbol{\Delta}_i = \begin{Bmatrix} v_0 \\ w_f \\ \theta \\ \beta_f \\ \beta_r \end{Bmatrix}_i, \tag{12a}$$

$$\mathbf{N}(y) = \begin{bmatrix} \mathbf{N}_1(\xi) & \mathbf{N}_2(\xi) & \mathbf{N}_3(\xi) \end{bmatrix}, \mathbf{N}_i(\xi) = N_i(\xi)\mathbf{I}, \quad i = 1,2,3,$$

where $\boldsymbol{\Delta}_i$, $i = 1,2,3$, are the sub-vectors of nodal displacements corresponding to the three points within the element, $\mathbf{I}$ is a 5×5 unit matrix and $N_i(\xi)$, $i = 1,2,3$,are quadratic interpolation functions defined by

$$N_1(\xi) = 2(\xi-1)(\xi-\frac{1}{2}),\ N_2(\xi) = -4\xi(\xi-1),\ N_3(\xi) = 2\xi(\xi-\frac{1}{2}),$$
$$0 \le \xi = \frac{y_e}{\ell_e} \le 1, \tag{12b}$$

in which ℓ_e is the length of the element and ξ is the natural local non-dimensional coordinate starting from node 1 of the element denoted in Fig. 3.

Substituting Eq. (11) into Eq. (8), we get the Lagrangian function in single element

$$\Pi - T = \frac{1}{2}\mathbf{u}_e^T[g^2(t)\mathbf{K}_e - \dot{g}^2(t)\mathbf{J}_e]\mathbf{u}_e - g(t)\mathbf{u}_e^T\mathbf{f}_e, \tag{13a}$$

where $\mathbf{K}_e$, $\mathbf{J}_e$, and $\mathbf{f}_e$ are, respectively, the *element stiffness matrix*, *element inertia matrix*, and *element force vector*, and are defined as

$$\begin{aligned}
\mathbf{K}_e &= \int_0^1 \left\{ \mathbf{N}^T(\xi)\mathbf{K}_0\mathbf{N}(\xi) + 2\mathbf{N}^T(\xi)\mathbf{K}_1^T\mathbf{N}'(\xi) + \mathbf{N}'^T(\xi)\mathbf{K}_2\mathbf{N}'(\xi) \right\} \ell_e d\xi, \\
\mathbf{J}_e &= \int_0^1 \left\{ \mathbf{N}^T(\xi)\mathbf{I}_0\mathbf{N}(\xi) \right\} \ell_e d\xi, \\
\mathbf{f}_e &= \int_0^1 \left\{ \mathbf{N}^T(\xi)\mathbf{p}(\xi) \right\} \ell_e d\xi + [\mathbf{N}^T(\xi)\hat{\mathbf{F}}(\xi)]_0^1.
\end{aligned} \tag{13b}$$

By substituting Eq. (12) into Eq. (13b) and assuming uniform pressure with constant load vector $\mathbf{p}$ within each element, the explicit forms of the element stiffness matrix, inertia matrix, and element force vector can be obtained as

$$\begin{aligned}
\mathbf{K}_e =& \ell_e \begin{bmatrix} \frac{2}{15}\mathbf{K}_0 & \frac{1}{15}\mathbf{K}_0 & -\frac{1}{30}\mathbf{K}_0 \\ \frac{1}{15}\mathbf{K}_0 & \frac{8}{15}\mathbf{K}_0 & \frac{1}{15}\mathbf{K}_0 \\ -\frac{1}{30}\mathbf{K}_0 & \frac{1}{15}\mathbf{K}_0 & \frac{2}{15}\mathbf{K}_0 \end{bmatrix} + \begin{bmatrix} -\frac{1}{2}\mathbf{K}_1^T & \frac{2}{3}\mathbf{K}_1^T & -\frac{1}{6}\mathbf{K}_1^T \\ -\frac{2}{3}\mathbf{K}_1^T & 0\mathbf{K}_1^T & \frac{2}{3}\mathbf{K}_1^T \\ \frac{1}{6}\mathbf{K}_1^T & -\frac{2}{3}\mathbf{K}_1^T & \frac{1}{2}\mathbf{K}_1^T \end{bmatrix} \\
&+ \frac{1}{\ell_e} \begin{bmatrix} \frac{7}{3}\mathbf{K}_2 & -\frac{8}{3}\mathbf{K}_2 & \frac{1}{3}\mathbf{K}_2 \\ -\frac{8}{3}\mathbf{K}_2 & \frac{16}{3}\mathbf{K}_2 & -\frac{8}{3}\mathbf{K}_2 \\ \frac{1}{3}\mathbf{K}_2 & -\frac{8}{3}\mathbf{K}_2 & \frac{7}{3}\mathbf{K}_2 \end{bmatrix}
\end{aligned}$$

$$\mathbf{J}_e = \ell_e \begin{bmatrix} \frac{2}{15}\mathbf{I}_0 & \frac{1}{15}\mathbf{I}_0 & -\frac{1}{30}\mathbf{I}_0 \\ \frac{1}{15}\mathbf{I}_0 & \frac{8}{15}\mathbf{I}_0 & \frac{1}{15}\mathbf{I}_0 \\ -\frac{1}{30}\mathbf{I}_0 & \frac{1}{15}\mathbf{I}_0 & \frac{2}{15}\mathbf{I}_0 \end{bmatrix}, \quad \mathbf{f}_e = \ell_e \begin{Bmatrix} \frac{1}{6}\mathbf{p} \\ \frac{2}{3}\mathbf{p} \\ \frac{1}{6}\mathbf{p} \end{Bmatrix} + \begin{Bmatrix} -\hat{\mathbf{F}}(0) \\ 0 \\ \hat{\mathbf{F}}(1) \end{Bmatrix}. \tag{14}$$

Note that $\mathbf{K}_e$, $\mathbf{J}_e$, and $\mathbf{f}_e$ calculated from Eq. (14) will have different values for different elements if a tapered wing is considered, since $\mathbf{K}_0$, $\mathbf{K}_1$, $\mathbf{K}_2$, and $\mathbf{I}_0$ defined in Eq. (3b,c) are related to the chord length of element which is a function of spanwise location, i.e., $c = c(y)$. And the dimensions of $\mathbf{K}_e$, $\mathbf{J}_e$, and $\mathbf{f}_e$ are, respectively, 15×15, 15×15, and 15×1.

4 Static Analysis

The foregoing model is general enough to deal with both static and dynamic analysis in tapered composite wings. If we only consider the static model, the function $g(t)$ should be independent of time and can be set as $g(t) = 1$. With this substitution, Eq. (13) can be rewritten as

$$\Pi = \frac{1}{2}\mathbf{u}_e^T\mathbf{K}_e\mathbf{u}_e - \mathbf{u}_e^T\mathbf{f}_e. \tag{15}$$

By taking the first variation of the total potential energy Π to be zero, the equilibrium equation within a single element can be obtained as

$$\frac{1}{2}\left(\mathbf{K}_e+\mathbf{K}_e^T\right)\mathbf{u}_e=\mathbf{f}_e. \tag{16}$$

Once we divide the wing into n elements, there are $2n$+1 nodes in structure. Because there is a common node shared by two adjacent elements, the total number of the common nodes of the wing structure will be n-1. As every nodal displacement sub-vector $\mathbf{\Delta}_i$ contains five components (v_0, w_f, θ, β_f, and β_r), the dimension of the global nodal displacement vector $\mathbf{u}_g$ becomes (10n+5) $\times$1. The global stiffness matrix $\mathbf{K}_g$ is a (10n+5) $\times$ (10n+5) matrix and the global force vector $\mathbf{f}_g$ is a (10n+5) $\times$ 1 vector. With the concept of finite element method, we can move all the element stiffness and force vectors into the corresponding position in global ones. The portions related to the common nodes between two elements will overlap. The global stiffness matrices $\mathbf{K}_g$ and force vector $\mathbf{f}_g$ are further fulfilled by superimposing all the values of the element stiffness matrices and force vectors, and finally the equilibrium equation for the entire wing structures can be written as follows

$$\frac{1}{2}\left(\mathbf{K}_g+\mathbf{K}_g^T\right)\mathbf{u}_g=\mathbf{f}_g. \tag{17}$$

Equation (17) is a standard form of the system of linear algebraic equations. With the known values of $\mathbf{K}_g$ and the prescribed values of $\mathbf{f}_g$ or $\mathbf{u}_g$ set for the problems, all the unknowns $\mathbf{u}_g$ or $\mathbf{f}_g$ can be solved in principle. Typical numerical examples using the present model for static analysis will be shown in Section 6.

5 Free Vibration

In this section, free vibration of the tapered wing structure is considered. The pressure $\mathbf{p}$ and nodal force $\hat{\mathbf{F}}$ are both set to be zero, and hence the element force vector $\mathbf{f}_e=\mathbf{0}$. A harmonic motion is assumed for free vibration analysis, i.e., $g(t)=e^{i\omega t}$ where ω is the natural frequency. With these assumptions, the Lagrangian function in Eq. (13) can be reduced to

$$\Pi-T=\frac{e^{2i\omega t}}{2}\mathbf{u}_e^T[\mathbf{K}_e+\omega^2\mathbf{J}_e]\mathbf{u}_e. \tag{18}$$

By taking the first variation of the Lagrangian function $\Pi-T$ to be zero, the equation of motion for a single element can be derived as

$$\frac{1}{2}\left[\left(\mathbf{K}_e+\mathbf{K}_e^T\right)+\omega^2\left(\mathbf{J}_e+\mathbf{J}_e^T\right)\right]\mathbf{u}_e=\mathbf{0}. \tag{19}$$

Following the standard procedure for element assembly, the global stiffness matrix $\mathbf{K}_g$, the global inertia matrix $\mathbf{J}_g$, and global force vector $\mathbf{f}_g$ can be obtained, and the equation of motion for the entire wing structures can be written as

$$\frac{1}{2}\left[\left(\mathbf{K}_g+\mathbf{K}_g^T\right)+\omega^2\left(\mathbf{J}_g+\mathbf{J}_g^T\right)\right]\mathbf{u}_g=\mathbf{0}. \tag{20}$$

Equation (20) is a typical form of eigenvalue problem which contains (10n+5) eigenvalue equations where ω^2 and $\mathbf{u}_g$ are eigenvalues and eigenvectors, respectively. After embedding the boundary conditions, the system of equations (20) will be reduced. The natural frequency ω can then be solved by letting the determinant of the reduced coefficient matrix of $\mathbf{u}_g$ be zero. The mode shape $\mathbf{u}_g$ corresponding to the natural frequency ω is obtained via Eq. (20).

6 Numerical Results and Discussion

In order to investigate the correctness, efficiency, and applicability of the proposed comprehensive finite element model, several numerical examples of composite wing structures are presented in this section. They are: (1) uniform wings subjected to end load, (2) tapered wings subjected to end load, (3) tapered wings subjected to uniform pressure, (4) free vibration of uniform wings, and (5) free vibration of tapered wings. The convergence test and its related comparison of computational efficiency between the present model and the finite element software ANSYS are presented through the first example for static analysis. Further comparison with ANSYS is done in example 4 for free vibration analysis, and the accuracy of the present model is verified through the analytical solution for uniform wing structures. The applicability to tapered wings is then shown in examples 2 and 3 for static case and example 5 for free vibration analysis. The taper effect is studied by varying the tapered ratio r_t defined as $r_t = c_t/c_r$, where c_t and c_r are, respectively, the chord length at wing tip and wing root. The uniform wings in our examples mean that the wing cross section is uniform in the spanwise direction, i.e., the chord length $c(y)$ which is supposed to be a function of y for tapered wings is now a constant for uniform wings.

All the examples in our studies consider the composite wing structure with NACA 2412 airfoil. From the data given in [Hunsaker (1949)], the shape of airfoil is approximated by a 9^{th}-order polynomial as

$$\begin{aligned} f_u(\bar{x})/c &= 0.0719-0.0588\bar{x}-0.0769\bar{x}^2-0.767\bar{x}^3-2.599\bar{x}^4+15.382\bar{x}^5 \\ &\quad +18.536\bar{x}^6-92.174\bar{x}^7-45.673\bar{x}^8+186.078\bar{x}^9, \\ f_u(\bar{x})/c &= -0.0329+0.0405\bar{x}-0.0239\bar{x}^2+0.675\bar{x}^3+1.815\bar{x}^4-12.310\bar{x}^5 \\ &\quad -13.870\bar{x}^6+73.449\bar{x}^7+36.096\bar{x}^8-149.862\bar{x}^9,\ \bar{x}=x/c, \end{aligned} \tag{21}$$

where $f_u(\bar{x})$ and $f_l(\bar{x})$ are respectively the approximate functions for the upper and lower surfaces of the airfoil in which the coordinate origin is located at the mid-point of the chord line. The chordwise length c=0.1m at wing root and varies linearly along the spanwise direction according to the tapered ratio. The wing spanwise length is fixed at L=0.4m for all examples unless stated otherwise. The wing skin is made of graphite/epoxy fiber-reinforced composite whose mechanical properties are: E_L= 200 GPa, E_T= 5 GPa, ν_{LT} = 0.25, G_{LT}= 2.5GPa, $\rho = 1.9$ g / cm^3, and ply thickness t = 0.025 mm. The laminate layup is [90 / - 45 / 45 / 0] for upper skin and [0 / 45 / - 45 / 90] for lower skin. Two wing spars made of isotropic materials with shear modulus $G = 8$ GPa and thickness 0.6 mm are located at $\pm 0.25c$ from the mid-chord line. Eight stringers and two ribs, made of Aluminum with material properties E = 69 GPa, ν = 0.33, $G = 26$ GPa, and $\rho = 2.8$ g / cm^3, are equally-spaced on the wing. The thickness of the pseudolamina constructed by stringers and ribs was set as 1.5 mm.

Example 1: uniform wings subjected to end load

In this case, the taper ratio is set to be unit, and a concentrated load $\tilde{Q}_y = 500$ N is applied at the wing tip. The wing is modeled as a cantilever with fixed end at wing root, and is meshed into several elements like that shown in Fig. 3. To show the convergence rate of the present model and the other existing finite element model such as ANSYS, the deflection w_f at wing tip versus number of elements is shown in Tab. 1. In the modeling process of ANSYS, SHELL91 element is used to construct the wing skins and a series of solid elements such as SOLID185, SOLID95, and SOLID187 are chosen to model the core of the wing. From Tab. 1 we see that the differences of the convergent values between the present model and those of ANSYS are within 10%. Only 4 elements are used to get the convergent results of the present model, while more than 582 elements are needed for ANSYS. This case is carried out by the Intel(R) Core(TM)2 Duo E8500 (3.16GHz) personal computer within 9 seconds using the present model, while 113 seconds with ANSYS, which leads to 92% saving of the computational time.

Since the convergent study has been presented in this example, without further statements in the following examples all the results are shown with the convergent values. Moreover, since in ANSYS the performance of SHELL91 plus SOLID95 is better than the others for wing analysis, when we mention the results analyzed by ANSYS in the following examples it means that the comparison results were implemented by ANSYS with SHELL91 for wing skins and SOLID95 elements for wing cores.

Example 2: tapered wings subjected to end load

To see the applicability of the present model to tapered composite wings, the taper

Table 1: Convergence test of finite element modeling

Present							
Number of Elements	1	2	4	8	40	100	200
Wing tip deflection, m	0.1583	0.1913	0.1968	0.1974	0.1974	0.1974	0.1974
ANSYS, SOLID 185							
Number of Elements	907	2180	4001	6456	9574	17656	23418
Wing tip deflection, m	0.0898	0.1582	0.2137	0.2310	0.2296	0.2244	0.2202
ANSYS, SOLID 95							
Number of Elements	101	234	582	904	2175	7686	25109
Wing tip deflection, m	0.2081	0.1959	0.1839	0.1844	0.1822	0.1843	0.1838
ANSYS, SOLID 187							
Number of Elements	904	2175	4003	6456	7711	10255	25094
Wing tip deflection, m	0.1022	0.1501	0.1649	0.1741	0.1765	0.1802	0.1837

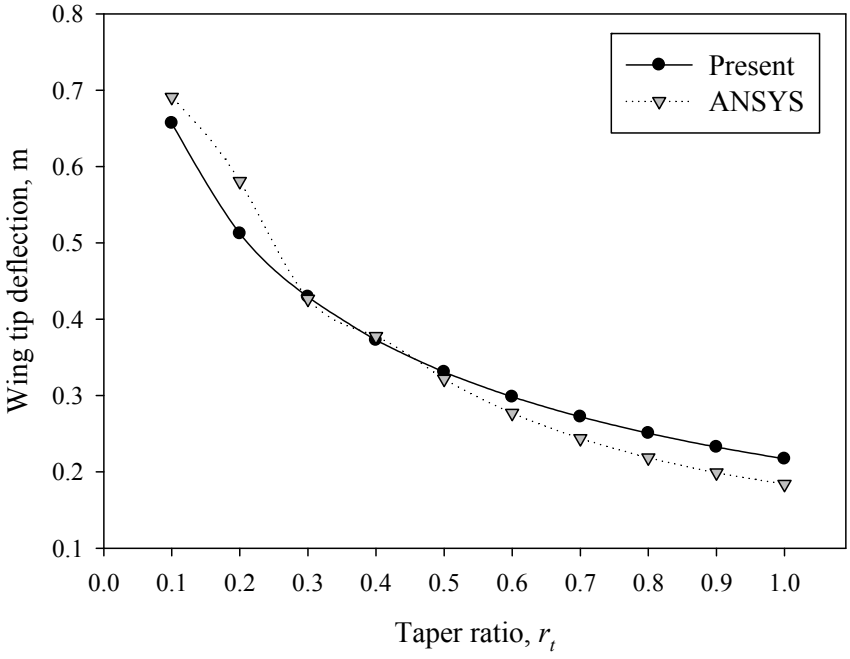

Figure 4: Wing tip deflection vs. taper ratio for the case of end load.

ratio of example 1 is now varied from 0.1 to 1. The convergent results of wing tip deflection versus taper ratio are presented in Fig. 4, which show that the deflection w_f decreases when the taper ratio increases. From this figure we see that the differences between the present model and those of ANSYS are within 11%, which are acceptable.

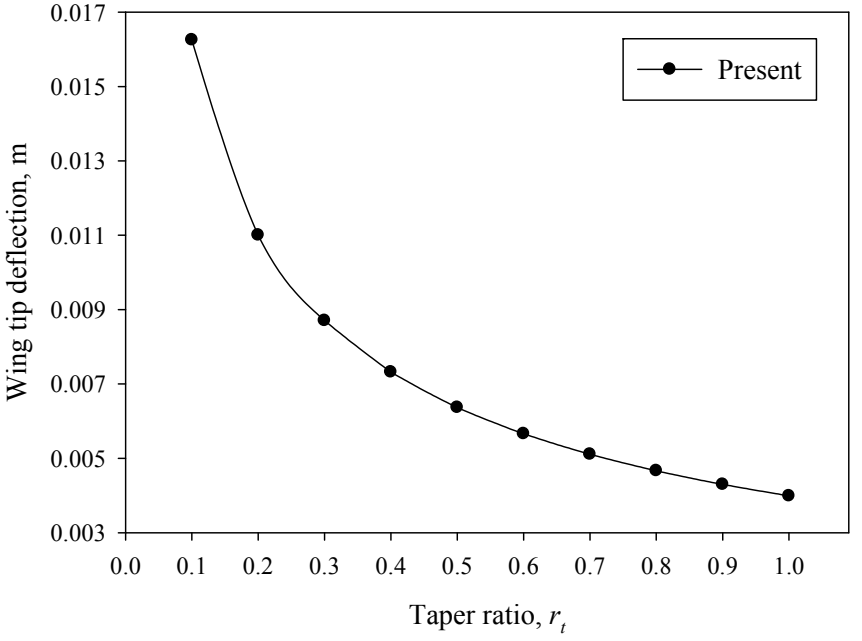

Figure 5: Wing tip deflection vs. taper ratio for the case of uniform pressure.

Example 3: tapered wings subjected to uniform pressure

From the last equation of (14) we know that the element force vector $\mathbf{f}_e$ is related to both of the nodal force $\hat{\mathbf{F}}$ and the pressure $\mathbf{p}$. To show that the present model can also deal with the wings subjected to distributed pressure on wing skins, in this example a uniform pressure $\tilde{p}$ of 1250 N/m is applied on the upper skin of the wing. Fig. 5 shows the trend of the deflection w_f versus taper ratio is similar to that of end load considered in Example 2.

Example 4: free vibration of uniform wings

The analytical solution of natural frequencies for composite wings was obtained in our previous work [Hwu and Gai (2003)], which is valid only for uniform wings.

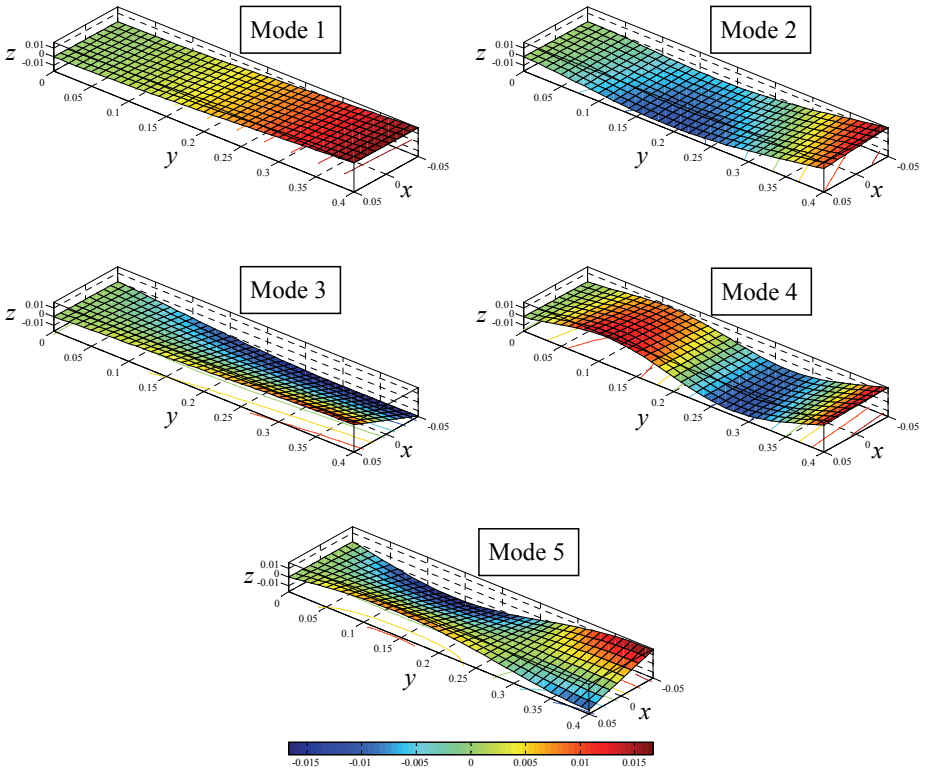

Figure 6: Mode shapes of the first five vibration modes.

To check the correctness of the present comprehensive finite element model, the natural frequencies of uniform wings are calculated by using the present model, the analytical solution, and ANSYS. Tab. 2 shows the comparison of natural frequencies. Their associated mode shapes are plotted in Fig. 6. All these results show that they well agree with each other, and their differences are within 12%. Like the convergent studies presented in Example 1, by the Intel(R) Core(TM)2 Duo E8500 (3.16GHz) personal computer this case is carried out within 55 seconds using the present model, while 690 seconds using analytical solutions, and 910 seconds with ANSYS. In other words, the calculating time of the present model is only 8% and 6% of the time consumed by the analytical model and ANSYS, respectively.

Example 5: free vibration of tapered wings

In this example, the taper ratio is varied from 0.2 to 1. The results and comparison of the fundamental natural frequencies versus taper ratio are shown in Fig. 7, and

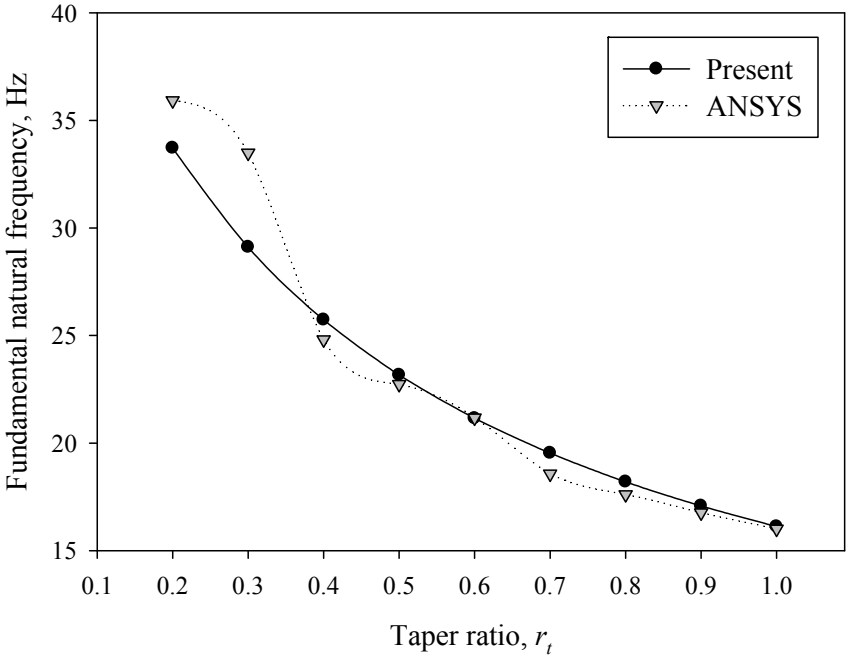

Figure 7: Fundamental natural frequency vs. taper ratio.

the natural frequencies of the first five modes are shown in Fig. 8. The comparison with ANSYS presented in Fig. 7 shows that most of the results agree well each other, except the range for r_t = 0.2-0.3, which may come from the inappropriate mesh process induced by the abruptly change of geometric variation. From Fig. 7 and Fig. 8 we see that most of the natural frequencies increase when the taper ratio r_t is reduced.

7 Conclusions

By Hamilton's principle, the matrix form comprehensive wing model is re-derived in this paper. With the aid of finite element technique, the comprehensive wing model is further extended to the comprehensive finite element model and is applicable to the tapered composite wing structures. The present model is a one-dimensional model and thus is like a beam element, but it contains 5 degrees of freedom in each node and performs like a solid element. Through the numerical studies of static and free vibration cases shown in Section 6, it has been shown that

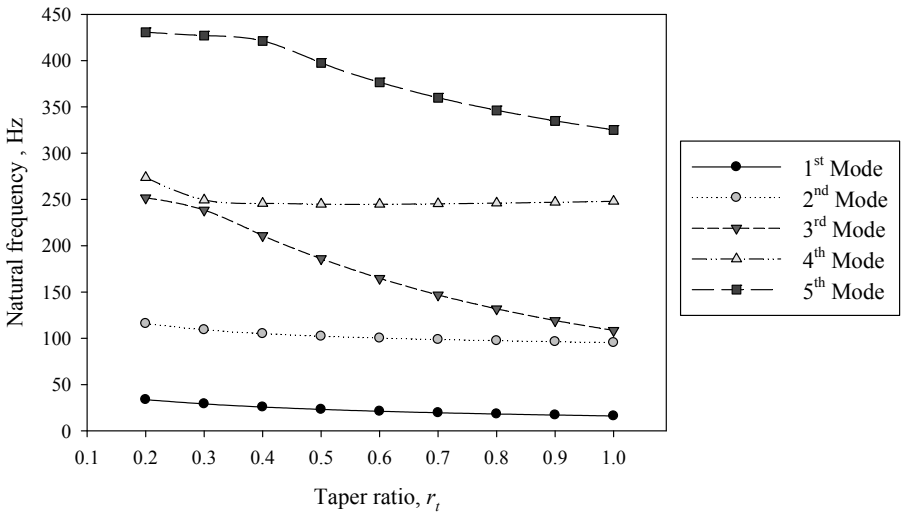

Figure 8: Natural frequencies of the first five modes vs. taper ratio.

Table 2: Natural frequencies of uniform wings

Frequency, Hz					
Method	Mode 1	Mode 2	Mode 3	Mode 4	Mode 5
		Span Length, L = 0.4m			
Present	16.12	95.33	108.40	248.00	325.03
Analytical[Hwu and Gai (2003)]	16.15	96.45	110.34	252.45	333.85
ANSYS	16.66	99.72	118.57	264.31	357.92
		Span Length, L = 0.3m			
Present	28.45	142.83	164.19	399.78	439.08
Analytical[Hwu and Gai (2003)]	28.51	148.04	164.83	414.21	450.71
ANSYS	27.90	154.10	160.47	403.10	459.12
		Span Length, L = 0.2m			
Present	62.72	215.30	330.37	645.01	765.02
Analytical[Hwu and Gai (2003)]	62.97	225.69	335.69	690.42	788.67
ANSYS	61.88	233.57	326.95	686.14	765.56

the present model is really accurate and efficient. The results for tapered wings show that the larger the taper ratio the smaller the vertical deflection and natural frequencies.

Acknowledgement: The authors would like to thank the support by National Science Council through grant NSC 96-2221-E-006-174.

Appendix A: Definition of some symbols used in this paper

(i) *Applied loads* $\tilde{p}_y, \tilde{p}, \tilde{m}_x - \tilde{p}^*, \tilde{m}_y, \tilde{m}_y^*$:

$$\begin{aligned} &\tilde{p}_y = \int_{-c/2}^{c/2} p_y dx,\ \tilde{p} = \int_{-c/2}^{c/2} p dx,\ \tilde{m}_x = \int_{-c/2}^{c/2} m_x dx,\ \tilde{m}_y = \int_{-c/2}^{c/2} m_y dx, \\ &\tilde{p}^* = \int_{-c/2}^{c/2} p x dx,\ \tilde{m}_y^* = \int_{-c/2}^{c/2} m_y x dx, \end{aligned} \tag{A1}$$

where p_y, p and m_x, m_y are the distributed loads of y, z direction and moments of x, y direction applied on the upper and/or lower surfaces of the composite wings.

(ii) *Resultant forces* $\tilde{N}_y$, $\tilde{Q}_y$, $\tilde{M}_{xy}$, $\tilde{M}_y$, $\tilde{Q}_y^*$, $\tilde{M}_y^*$:

$$\begin{aligned} &\tilde{N}_y = \int_{-c/2}^{c/2} N_y dx,\ \tilde{Q}_y = \int_{-c/2}^{c/2} Q_y dx,\ \tilde{M}_{xy} = \int_{-c/2}^{c/2} M_{xy} dx,\ \tilde{M}_y = \int_{-c/2}^{c/2} M_y dx, \\ &\tilde{Q}_y^* = \int_{-c/2}^{c/2} Q_y x dx,\ \tilde{M}_y^* = \int_{-c/2}^{c/2} M_y x dx, \end{aligned} \tag{A2}$$

where N_y, Q_y and M_{xy}, M_y are the stress resultants defined by

$$\begin{Bmatrix} N_x \\ N_y \\ N_{xy} \end{Bmatrix} = \int_{-h/2}^{h/2} \begin{Bmatrix} \sigma_x \\ \sigma_y \\ \tau_{xy} \end{Bmatrix} dz,\ \begin{Bmatrix} M_x \\ M_y \\ M_{xy} \end{Bmatrix} = \int_{-h/2}^{h/2} \begin{Bmatrix} \sigma_x \\ \sigma_y \\ \tau_{xy} \end{Bmatrix} z dz,\ \begin{Bmatrix} Q_x \\ Q_y \end{Bmatrix} = \int_{-h/2}^{h/2} \begin{Bmatrix} \tau_{xz} \\ \tau_{yz} \end{Bmatrix} dz. \tag{A3}$$

(iii) *Mass* m, *center of gravity* (x_c, z_c) and *moment of inertia* $I_x, I_y, I_{xz}, I_{xz^2}$, and $I_{x^2z^2}$:

$$\begin{aligned} &m = \int_A \rho dA,\ mx_c = \int_A \rho x dA,\ mz_c = \int_A \rho z dA, \\ &I_x = \int_A \rho z^2 dA,\ I_y = \int_A \rho (x^2 + z^2) dA, \\ &I_{xz} = \int_A \rho xz dA,\ I_{xz^2} = \int_A \rho x z^2 dA,\ I_{x^2z^2} = \int_A \rho x^2 z^2 dA, \end{aligned} \tag{A4}$$

where ρ is the mass density and A is the area of chordwise cross section.
(iv) *Resultant stiffness* $\tilde{A}_{ij},\tilde{B}_{ij},\tilde{D}_{ij},\tilde{A}^*_{ij},\tilde{B}^*_{ij},\tilde{D}^*_{ij},\tilde{A}^{**}_{ij},\tilde{B}^{**}_{ij},\tilde{D}^{**}_{ij}$:

$$\begin{aligned}
&\tilde{A}_{ij}=\int_{-c/2}^{c/2}A_{ij}dx,\ \ \tilde{B}_{ij}=\int_{-c/2}^{c/2}B_{ij}dx,\ \ \tilde{D}_{ij}=\int_{-c/2}^{c/2}D_{ij}dx,\\
&\tilde{A}^*_{ij}=\int_{-c/2}^{c/2}A_{ij}xdx,\ \ \tilde{B}^*_{ij}=\int_{-c/2}^{c/2}B_{ij}xdx,\ \ \tilde{D}^*_{ij}=\int_{-c/2}^{c/2}D_{ij}xdx,\\
&\tilde{A}^{**}_{ij}=\int_{-c/2}^{c/2}A_{ij}x^2dx,\ \ \tilde{B}^{**}_{ij}=\int_{-c/2}^{c/2}B_{ij}x^2dx,\ \ \tilde{D}^{**}_{ij}=\int_{-c/2}^{c/2}D_{ij}x^2dx,\ \ i,\ j=1,2,...,6,
\end{aligned} \tag{A5}$$

where the integration limits $\pm c/2$ are the two ends of chord whose length is c. A_{ij}, B_{ij} and D_{ij} are, respectively, the extensional, coupling, and bending stiffnesses of the composite wings which are defined by

$$\begin{aligned}
&A_{44}=\alpha h G_{yz},\ A_{ij}=\sum_{k=1}^{n}(\overline{Q}_{ij})_k(z_k-z_{k-1}),\\
&B_{ij}=\frac{1}{2}\sum_{k=1}^{n}(\overline{Q}_{ij})_k(z_k^2-z_{k-1}^2),\ D_{ij}=\frac{1}{3}\sum_{k=1}^{n}(\overline{Q}_{ij})_k(z_k^3-z_{k-1}^3),\ i,j=1,2,6.
\end{aligned} \tag{A6}$$

In the above, $h$is the thickness of the wing cross-section and is a function of x; G_{yz} is the transverse shear modulus in $y-z$ plane; α is the transverse shear correction factor and is selected to be 5/6 for the present case [Cowper (1966)]. $(\overline{Q}_{ij})_k$ are the transformed reduced stiffnesses of the kth lamina; z_k and z_{k-1} denote, respectively, the location of the bottom and top surfaces of the kth lamina.

Note that in the calculation of A_{ij}, B_{ij}, and D_{ij}, not only the composite laminates of the faces are counted but also the stringers and spar flanges which are considered to be the fibers of a pseudo-lamina. The equivalent material properties of this pseudo-lamina can be found by the rule of mixture as [Hwu and Tsai (2002)]

$$E_L=E_s\frac{A_s}{A_p}+E_f\frac{A_f}{A_p},\ \nu_{LT}=\nu_s\frac{A_s}{A_p}+\nu_f\frac{A_f}{A_p},\ E_T=0,\ G_{LT}=0, \tag{A7}$$

where E, ν, G, and A denote, respectively, the Young's modulus, Poisson's ratio, shear modulus, and cross-section area. The subscript L, T, s, and f denote the longitudinal direction, transverse direction, stringer, and spar flange, respectively. A_p stands for the cross section area of pseudo-lamina.

In order to find a proper transverse shear modulus G_{yz} that may represent the shear resistance of the multicellular wing structures, the arrangement of the wing spar

webs and ribs can be treated like a sandwich honeycomb core. By assuming uniform transverse shear strain over the wing cross section, the equivalent transverse shear modulus G_{yz} can be estimated by [Hwu and Tsai (2002)]

$$G_{yz} = \sum_{k=1}^{n_s} G_k A_k / A_w \tag{A8}$$

where G_k and A_k denote the shear modulus and section area of the kth spar web, A_w is the wing cross section area and n_s is the number of the wing spars.

Appendix B: Integration of potential and kinetic energy

If the integral is performed in the sequence of thickness direction (z), chordwise direction (x), and spanwise direction (y), each term of the potential and kinetic energy shown in Eq. (5) can be integrated as follows.

$$\begin{aligned}
&\int_V W dV \\
&= \frac{1}{2}\int_V \sigma_{ij}\varepsilon_{ij} dV \\
&= \frac{1}{2}\int_A \{N_x\varepsilon_{x_0} + N_y\varepsilon_{y_0} + N_{xy}\gamma_{xy_0} + M_x\kappa_x + M_y\kappa_y + M_{xy}\kappa_{xy} + Q_x\gamma_{xz} + Q_y\gamma_{yz}\} dxdy \\
&= \frac{1}{2}\int_A \{N_y(v_0') + M_y(\beta_f' + x\beta_r') + M_{xy}(\beta_r + \theta') + Q_y[\beta_f + w_f' + x(\beta_r - \theta')]\} dxdy \\
&= \frac{1}{2}\int_y \{\tilde{N}_y v_0' + \tilde{M}_y\beta_f' + \tilde{M}_y^*\beta_r' + \tilde{M}_{xy}(\beta_r + \theta') + \tilde{Q}_y(\beta_f + w_f') + \tilde{Q}_y^*(\beta_r - \theta')\} dy \\
&= \frac{1}{2}\int_y \{\mathbf{F}^T\boldsymbol{\Delta}' + \mathbf{F}_0^T\boldsymbol{\Delta}\} dy
\end{aligned} \tag{B1}$$

$$\begin{aligned}
\int_V f_i u_i dV &= \int_A \{p_x u + p_y v + pw\} dxdy \\
&= \int_A \{p_x(z\theta) + p_y[v_0 + z(\beta_f + x\beta_r)] + p(w_f - x\theta)\} dxdy \\
&= \int_A \{m_x\theta + p_y v_0 + m_y(\beta_f + x\beta_r) + p(w_f - x\theta)\} dxdy \\
&= \int_y \{\tilde{m}_x\theta + \tilde{p}_y v_0 + \tilde{m}_y\beta_f + \tilde{m}_y^*\beta_r + \tilde{p}w_f - \tilde{p}^*\theta\} dy \\
&= \int_y \{\mathbf{p}^T\boldsymbol{\Delta}\} dy
\end{aligned} \tag{B2}$$

$$\begin{aligned}\int_{S_\sigma} \hat{t}_i u_i dS &= \left[\int_x \{\hat{M}_{xy}\theta + \hat{N}_y v_0 + \hat{M}_y(\beta_f + x\beta_r) + \hat{Q}_y(w_f - x\theta)\}dx\right]_{y_r}^{y_t} \\ &= \left[\hat{\hat{M}}_{xy}\theta + \hat{\hat{N}}_y v_0 + \hat{\hat{M}}_y\beta_f + \hat{\hat{M}}_y^*\beta_r + \hat{\hat{Q}}_y w_f - \hat{\hat{Q}}_y^*\theta\right]_{y_r}^{y_t} \\ &= [\hat{\mathbf{F}}^T\boldsymbol{\Delta}]_{y_r}^{y_t}\end{aligned} \tag{B3}$$

$$\begin{aligned}\frac{1}{2}\int_V \rho\dot{u}_i\dot{u}_i dV &= \frac{1}{2}\int_V \rho\{\dot{u}^2 + \dot{v}^2 + \dot{w}^2\}dV \\ &= \frac{1}{2}\int_V \rho\{(z\dot{\theta})^2 + (\dot{v}_0 + z\dot{\beta}_f + zx\dot{\beta}_r)^2 + (\dot{w}_f - x\dot{\theta})^2\}dzdxdy \\ &= \frac{1}{2}\int_y \{I_x(\dot{\theta}^2 + \dot{\beta}_f^2) + I_z\dot{\theta}^2 + 2I_{xz}\dot{v}_0\dot{\beta}_r + 2I_{xz^2}\dot{\beta}_f\dot{\beta}_r + I_{x^2z^2}\dot{\beta}_r^2 \\ &\quad + m(\dot{v}_0^2 + \dot{w}_f^2) - 2mx_c\dot{w}_f\dot{\theta} + 2mz_c\dot{v}_0\dot{\beta}_f\}dy \\ &= \frac{1}{2}\int_V \{\dot{\boldsymbol{\Delta}}^T\mathbf{I}_0\dot{\boldsymbol{\Delta}}\}dV\end{aligned} \tag{B4}$$

In Eq. (B1), $(\varepsilon_{x_0}, \varepsilon_{y_0}, \gamma_{xy_0})$ and $(\kappa_x, \kappa_y, \kappa_{xy})$ are the mid-plane strains and curvatures, and $(\gamma_{xz}, \gamma_{yz})$ are the transverse shear strain. With the displacement assumed in Eq. (1), we know that they are related to the basic functions $v_0,\ w_f,\ \theta,\ \beta_f$, and β_r by

$$\begin{aligned}&\varepsilon_{x_0} = 0,\ \varepsilon_{y_0} = v_0',\ \gamma_{xy_0} = 0 \\ &\kappa_x = 0,\ \kappa_y = \beta_f' + x\beta_r',\ \kappa_{xy} = \beta_r + \theta', \\ &\gamma_{xz} = 0,\ \gamma_{yz} = \beta_f + w_f' + x(\beta_r - \theta').\end{aligned} \tag{B5}$$

Appendix C: Variational operation

The variation of each term of Eq. (8) can be derived as follows.

$$\delta\int_y \boldsymbol{\Delta}^T\mathbf{K}_1^T\boldsymbol{\Delta}'dy = \int_y \delta\{\boldsymbol{\Delta}^T\mathbf{K}_1^T\boldsymbol{\Delta}'\}dy = \int_y \{(\delta\boldsymbol{\Delta}^T)\mathbf{K}_1^T\boldsymbol{\Delta}' + \boldsymbol{\Delta}^T\mathbf{K}_1^T\delta(\boldsymbol{\Delta}')\}dy \tag{C1}$$

in which the second term of the last equality can be rewritten as

$$\begin{aligned}&\int_y \boldsymbol{\Delta}^T\mathbf{K}_1^T\delta(\boldsymbol{\Delta}')dy = \int_y \boldsymbol{\Delta}^T\mathbf{K}_1^T(\delta\boldsymbol{\Delta})'dy = \int_y \{(\boldsymbol{\Delta}^T\mathbf{K}_1^T\delta\boldsymbol{\Delta})' - (\boldsymbol{\Delta}'^T\mathbf{K}_1^T\delta\boldsymbol{\Delta})\}dy \\ &= [\boldsymbol{\Delta}^T\mathbf{K}_1^T\delta\boldsymbol{\Delta}]_{y_r}^{y_t} - \int_y \boldsymbol{\Delta}'^T\mathbf{K}_1^T\delta\boldsymbol{\Delta}dy = [\boldsymbol{\Delta}^T\mathbf{K}_1^T\delta\boldsymbol{\Delta}]_{y_r}^{y_t} - \int_y (\delta\boldsymbol{\Delta}^T)\mathbf{K}_1\boldsymbol{\Delta}'dy.\end{aligned} \tag{C2}$$

Therefore,

$$\delta\int_y \boldsymbol{\Delta}^T\mathbf{K}_1^T\boldsymbol{\Delta}'dy = \int_y (\delta\boldsymbol{\Delta}^T)(\mathbf{K}_1^T - \mathbf{K}_1)\boldsymbol{\Delta}'dy + [(\delta\boldsymbol{\Delta})^T\mathbf{K}_1\boldsymbol{\Delta}]_{y_r}^{y_t}. \tag{C3}$$

Similarly,

$$\begin{aligned}
&\delta\int_y \boldsymbol{\Delta}'^T\mathbf{K}_2\boldsymbol{\Delta}'dy = -2\int_y(\delta\boldsymbol{\Delta}^T)\mathbf{K}_2\boldsymbol{\Delta}''dy + 2[(\delta\boldsymbol{\Delta}^T)\mathbf{K}_2\boldsymbol{\Delta}']_{y_r}^{y_t},\\
&\delta\int_y \boldsymbol{\Delta}^T\mathbf{K}_0\boldsymbol{\Delta}dy = 2\int_y(\delta\boldsymbol{\Delta}^T)\mathbf{K}_0\boldsymbol{\Delta}dy,\\
&\delta\int_y \dot{\boldsymbol{\Delta}}^T\mathbf{I}_0\dot{\boldsymbol{\Delta}}dy = -2\int_y(\delta\boldsymbol{\Delta}^T)\mathbf{I}_0\ddot{\boldsymbol{\Delta}}dy + 2\frac{\partial}{\partial t}\int_y(\delta\boldsymbol{\Delta}^T)\mathbf{I}_0\boldsymbol{\Delta}dy.
\end{aligned} \tag{C4}$$

References

Banerjee, J. R.; Williams, F. W. (1995): Free vibration of composite beams: an exact method using symbolic computation, *Journal of Aircraft*, vol. 32, no. 3, pp.636-642.

Bisplinghoff, R. L.; Asheley, H.; Halfman, R. L. (1955): *Aeroelasticity*. Addison-Wesley, Cambridge, MA, Chaps. 2 and 3.

Chandra, R.; Stemple, A. D.; Chopra, I. (1990): Thin-walled composite beams under bending, torsional, and extensional loads, *Journal of Aircraft*, vol. 27, pp.619-626.

Cowper, G. R. (1966): The Shear Coefficient in Timoshenko's Beam Theory, *Journal of Applied Mechanics*, vol. 3, no. 2, pp. 335-340.

Crawley, E. F.; Dugundji, J. (1980): Frequency determination and nondimensionalization for composite cantilever plates, *Journal of Sound and Vibration*, vol. 72, no. 1, pp. 1-10.

Hunsaker, J. C. (1949): *Theory of Wing Sections*, McGraw-Hill, New York, pp. 410.

Hwu, C.; Gai, H. S. (2003): Vibration analysis of composite wing structures by a matrix form comprehensive model, *AIAA Journal*, vol. 41, no. 11, pp.2261-2273.

Hwu, C.; Tsai, Z. S. (2002): Aeroelastic divergence of stiffened composite multicell wing structures, *Journal of Aircraft*, vol.39, no. 2, pp.242-251.

Librescu, L.; Khdeir, A.A. (1988): Aeroelastic divergence of swept-forward composite wings including warping restraint effect, *AIAA Journal*, vol. 26, no. 11, pp. 1373-1377.

Librescu, L.; Simovich, J. (1988): General formulation for the aeroelastic divergence of composite swept-forward wing structures, *Journal of Aircraft*, vol. 25, no. 4, pp.364-371.

Librescu, L.; Song, O. (1992): On the static aeroelastic tailoring of composite aircraft swept wings modelled as thin-walled beams structures, *Composite Engi-*

neering, Special Issue, Use of Composite in Rotor Craft and Smart Structures, vol. 2, no. 5-7, pp. 497-512.

Lottati, I. (1985): Flutter and divergence aeroelastic characteristics for composite forward swept cantilevered wing, *Journal of Aircraft*, vol. 22, no.11, pp. 1-10.

Megson, T. H. G. (1990): *Aircraft structures for engineering students*, 2nd ed., Edward Arnold, London, Chap. 8.

Oyibo, G. A.; Bentson, J. (1990): Exact solutions to oscillations of composite aircraft wings with warping constraint and elastic coupling, *AIAA Journal*, vol.28, no. 6, pp.1075-1081.

Reddy, J. N. (1993): *Applied functional analuysis and variational methods in engineering*, McGraw-Hill, New York.

Sapountzakis, E.J.; Tsiatas, G.C. (2007): Flexural-torsional buckling and vibration analysis of composite beams, *CMC: Computers, Material & Continua*, vol.6, no.2, pp.103-115

Vadiraja, D. N.; Sahasrabudhe, A. D. (2008): Vibration and control of rotating tapered thin-walled composite beam using macro fiber composite actuator, *CMES: Computer Modeling in Engineering & Sciences*, vol.27, no.1, pp.49-62

Vinod, K. G.; Gopalakrishnan, S.; Ganguli, R. (2006): Wave propagation characteristics of rotating uniform Euler-Bernoulli beams. *CMES: Computer Modeling in Engineering & Sciences*, vol.16, no.3, pp. 197-208

Volovoi, V. V.; Hodges, D. H. (2000): Theory of anisotropic thin-walled beams, *Journal of Applied Mechanics*, vol. 67, no. 3, pp. 453-459.

Volovoi, V. V.; Hodges, D. H. (2002): Single- and multicelled composite thin-walled beams, *AIAA Journal*, vol. 40, no. 5, pp. 960-965.

Weisshaar, T. A. (1980): Divergence of forward swept composite wings, *Journal of Aircraft*, vol. 17, no. 6, pp.442-448.

Weisshaar, T. A.; Foist, B. L. (1985): Vibration tailoring of advanced composite lifting surfaces, *Journal of Aircraft*, vol. 22, pp.141-147.

Yu, W.; Hodges, D. H.; Volovoi, V. V.; Cesnik, C.E.S. (2002): On Timoshenko-like modeling of initially curved and twisted composite beams, *International Journal of Solids and Structures*, vol. 39, pp. 5101-5121.

Yu, W.; Volovoi, V. V.; Hodges, D. H.; Hong, X. (2002): Validation of the variational asymptotic beam sectional analysis, *AIAA Journal*, vol. 40, no. 10, pp. 2105-2112.